J Seismol (2015) 19:231–252
DOI 10.1007/s10950-014-9463-y

ORIGINAL ARTICLE

Moment tensor decompositions revisited

Václav Vavryčuk

Received: 19 January 2014 / Accepted: 23 September 2014 / Published online: 16 October 2014

Abstract The decomposition of moment tensors into isotropic (ISO), double-couple (DC) and compensated linear vector dipole (CLVD) components is a tool for classifying and physically interpreting seismic sources. Since an increasing quantity and quality of seismic data allow inverting for accurate moment tensors and interpreting details of the source process, an efficient and physically reasonable decomposition of moment and source tensors is necessary. In this paper, the most common moment tensor decompositions are revisited, new equivalent formulas of the decompositions are derived, suitable norms of the moment tensors are discussed and the properties of commonly used source-type plots are analysed. The Hudson skewed diamond plot is introduced in a much simpler way than originally proposed. It is shown that not only the Hudson plot but also the diamond CLVD–ISO plot and the Riedesel–Jordan plot conserve the uniform distribution probability of moment eigenvalues if the appropriate norm of moment tensors is applied. When analysing moment tensor uncertainties, no source-type plot is clearly preferable. Since the errors in the eigenvectors and eigenvalues of the moment tensors cannot be easily separated, the moment tensor uncertainties project into the source-type plots in a complicated way. As a consequence, the moment tensors with the same uncertainties project into clusters of a different size. In case of an anisotropic focal area, the complexity of moment tensors of earthquakes prevents their direct interpretation, and the decomposition of moment tensors must be substituted by that of the source tensors.

Keywords Dynamics and mechanics of faulting · Earthquake source observations · Seismic anisotropy · Theoretical seismology

V. Vavryčuk (✉)
Institute of Geophysics, Academy of Sciences,
Boční II/1401, 14100 Praha 4, Czech Republic
e-mail: vv@ig.cas.cz

1 Introduction

The moment tensor describes equivalent body forces acting at a seismic point source (Burridge and Knopoff 1964) and is a basic quantity evaluated for earthquakes on all scales from acoustic emissions to large devastating earthquakes. The most common type of the moment tensor is the double-couple (DC) source which represents the force equivalent of shear faulting on a planar fault in isotropic media. However, many studies reveal that seismic sources often display more general moment tensors with significant non-double-couple (non-DC) components (Julian et al. 1998; Miller et al. 1998). An explosion is an obvious example of a non-DC source, but non-DC components can also be produced by the collapse of a cavity in mines (Rudajev and Šílený 1985; Šílený and Milev 2008), by shear faulting on a non-planar (curved or irregular) fault (Sipkin 1986), by tensile faulting induced by fluid injection in geothermal or volcanic areas (Ross et al. 1996; Julian et al. 1997) when the slip vector is inclined from the fault and causes its opening (Vavryčuk 2001, 2011) or by seismic anisotropy in the focal area (Kawasaki and Tanimoto 1981;

Vavryčuk 2005; Roessler et al. 2004, 2007). Complications also arise if the source is situated at a material interface (Vavryčuk 2013).

In order to identify which type of seismic source is physically represented by the retrieved moment tensor, Knopoff and Randall (1970) proposed decomposing the moment tensors into three elementary parts: the isotropic (ISO), double-couple (DC) and compensated linear vector dipole (CLVD) components. Although the moment tensor decomposition is not unique and many other decompositions have been proposed, the decomposition of Knopoff and Randall (1970) proved to be useful for physical interpretations and became widely accepted. This decomposition was further developed and applied by Sipkin (1986), Jost and Herrmann (1989), Hudson et al. (1989), Kuge and Lay (1994), Vavryčuk (2001, 2005, 2011) and others. Furthermore, Hudson et al. (1989) and Riedesel and Jordan (1989) proposed graphical representations of the DC and non-DC components in order to identify visually the most appropriate physical source corresponding to the retrieved moment tensor (for a geometric comparison of both approaches, see Tape and Tape 2012b).

Since an increasing quantity and quality of seismic data allow inverting for accurate moment tensors and interpreting the details of the source process, an efficient and physically reasonable decomposition of moment tensors is necessary. This has recently motivated several authors to revisit the existing decompositions (Chapman and Leaney 2012; Zhu and Ben-Zion 2013) and source-type plots (Chapman and Leaney 2012; Tape and Tape 2012a, b) and to develop their modifications. In this paper, I summarize the physical conditions imposed on the moment tensor decompositions and present new equivalent formulas for the most common moment tensor decompositions. I introduce the Hudson skewed diamond plot in a much simpler way than originally proposed. I compare several alternative moment tensor decompositions and source-type plots and discuss their advantages and drawbacks. I show differences in moment and source tensors (also called the potency tensors) and point out the significance of the source tensor decomposition for earthquake source interpretations in anisotropic media.

2 Orientation and type of source

The seismic moment tensor $\mathbf{M}$ is a symmetric tensor which can be decomposed using eigenvalues and an orthonormal basis of eigenvectors in the following way:

$$\mathbf{M} = M_1\mathbf{e}_1\mathbf{e}_1 + M_2\mathbf{e}_2\mathbf{e}_2 + M_3\mathbf{e}_3\mathbf{e}_3, \tag{1}$$

where

$$M_1 \geq M_2 \geq M_3 \tag{2}$$

and vectors $\mathbf{e}_1$, $\mathbf{e}_2$ and $\mathbf{e}_3$ define the T (tension), N (intermediate or neutral) and P (pressure) axes, respectively.

Using spectral decomposition (1), we separate two basic properties of the moment tensor: the orientation of the source defined by three eigenvectors, and the type and size of the source defined by three eigenvalues. Since the eigenvalues are independent, the type of the source can be represented as a point in three-dimensional (3-D) space (Riedesel and Jordan 1989)

$$\mathbf{m} = M_1\mathbf{e}_1 + M_2\mathbf{e}_2 + M_3\mathbf{e}_3, \tag{3}$$

where vectors $\mathbf{e}_1$, $\mathbf{e}_2$ and $\mathbf{e}_3$ define a coordinate system in this space. In order to get a unique representation, the eigenvalues must be ordered according to Eq. (2). Consequently, the points representing the source type cannot cover the whole 3-D space but only its wedge called the 'source-type space'. The choice of the coordinate system and the metric of the source-type space differ for individual moment tensor decompositions.

3 Standard moment tensor decomposition

3.1 Definition of ISO, DC and CLVD

In this decomposition, moment tensor $\mathbf{M}$ is diagonalized and further restructured to form three basic types of a source: the isotropic (ISO) and double-couple (DC) sources, which have a clear physical interpretation (see Section 3.3), and the compensated linear vector dipole (CLVD) source, which is needed for the decomposition to be mathematically complete (Knopoff and Randall 1970; Dziewonski et al. 1981; Sipkin 1986; Jost and Herrmann 1989; Hudson et al. 1989):

$$\begin{aligned}\mathbf{M} &= \mathbf{M}_{\mathrm{ISO}} + \mathbf{M}_{\mathrm{DC}} + \mathbf{M}_{\mathrm{CLVD}} \\ &= M_{\mathrm{ISO}}\mathbf{E}_{\mathrm{ISO}} + M_{\mathrm{DC}}\mathbf{E}_{\mathrm{DC}} + M_{\mathrm{CLVD}}\mathbf{E}_{\mathrm{CLVD}},\end{aligned} \tag{4}$$

where $\mathbf{E}_{\mathrm{ISO}}$, $\mathbf{E}_{\mathrm{DC}}$ and $\mathbf{E}_{\mathrm{CLVD}}$ are the ISO, DC and CLVD elementary tensors (also called the base tensors), and

M_{ISO}, M_{DC} and M_{CLVD} are the ISO, DC and CLVD coordinates in the 3-D source-type space. The elementary tensors read:

$$\mathbf{E}_{ISO} = \begin{bmatrix} 1 & 0 & 0 \\ 0 & 1 & 0 \\ 0 & 0 & 1 \end{bmatrix}, \quad (5)$$

$$\mathbf{E}_{DC} = \begin{bmatrix} 1 & 0 & 0 \\ 0 & 0 & 0 \\ 0 & 0 & -1 \end{bmatrix},$$

$$\mathbf{E}^{+}_{CLVD} = \frac{1}{2} \begin{bmatrix} 2 & 0 & 0 \\ 0 & -1 & 0 \\ 0 & 0 & -1 \end{bmatrix},$$

$$\mathbf{E}^{-}_{CLVD} = \frac{1}{2} \begin{bmatrix} 1 & 0 & 0 \\ 0 & 1 & 0 \\ 0 & 0 & -2 \end{bmatrix},$$

where $\mathbf{E}_{CLVD}$ is $\mathbf{E}^{+}_{CLVD}$ or $\mathbf{E}^{-}_{CLVD}$ depending on whether $M_1+M_3-2M_2 \geq 0$ or $M_1+M_3-2M_2<0$, respectively. Hence, the CLVD tensor is aligned along the axis with the largest magnitude deviatoric eigenvalue. The base tensors have ordered eigenvalues according to Eq. (2). This condition is needed for the base tensors to lie in the source-type space (i.e. in the space filled by moment tensors with ordered eigenvalues). The norm of all base tensors calculated as the largest magnitude eigenvalue (i.e. the maximum of $|M_i|$, $i=1,2,3$) is equal to 1. This condition is called the unit 'spectral norm' and physically means that the maximum dipole force of the base tensors is unity.

Equations (4) and (5) uniquely define values M_{ISO}, M_{DC} and M_{CLVD} expressed as follows:

$$M_{ISO} = \frac{1}{3}(M_1 + M_2 + M_3), \quad (6)$$

$$M_{CLVD} = \frac{2}{3}(M_1 + M_3 - 2M_2), \quad (7)$$

$$M_{DC} = \frac{1}{2}(M_1 - M_3 - |M_1 + M_3 - 2M_2|), \quad (8)$$

where M_{CLVD} also includes the sign of the elementary CLVD tensor. If the elementary CLVD tensor is considered with its sign as in Eq. (4), then M_{CLVD} should be calculated as the absolute value of Eq. (7).

In seismological practice, however, we do not evaluate values M_{ISO}, M_{DC} and M_{CLVD} in Eqs. (6–8) but rather scalar seismic moment M and relative scale factors C_{ISO}, C_{DC} and C_{CLVD} defined as:

$$\begin{bmatrix} C_{ISO} \\ C_{CLVD} \\ C_{DC} \end{bmatrix} = \frac{1}{M} \begin{bmatrix} M_{ISO} \\ M_{CLVD} \\ M_{DC} \end{bmatrix}, \quad (9)$$

where M reads

$$M = |M_{ISO}| + |M_{CLVD}| + M_{DC}, \quad (10)$$

and scale factors C_{ISO}, C_{DC} and C_{CLVD} satisfy the following equation:

$$|C_{ISO}| + |C_{CLVD}| + C_{DC} = 1. \quad (11)$$

Equations (6–10) imply that C_{DC} is always positive and in the range from 0 to 1; C_{CLVD} and C_{ISO} are in the range from −1 to 1. Consequently, the decomposition of **M** can be expressed as:

$$\mathbf{M} = M(C_{ISO}\mathbf{E}_{ISO} + C_{DC}\mathbf{E}_{DC} + |C_{CLVD}|\mathbf{E}_{CLVD}), \quad (12)$$

where M is the norm of **M** calculated using Eq. (10) and represents a scalar seismic moment for a general seismic source. The absolute value of the CLVD term in Eq. (12) is used because the sign of CLVD is included in the base tensor $\mathbf{E}_{CLVD}$. Equation (12) can be used also for composing **M** from known scale factors C_{ISO}, C_{DC} and C_{CLVD} and scalar moment M (see Appendix A).

Note that Eqs. (6–8) look different from those published by Jost and Herrmann (1989) but are equivalent. Also, Hudson et al. (1989) use different formulas and notation, but the resultant τ–k decomposition is the same as the CLVD–ISO decomposition except for the sign of the CLVD axis (for details, see Section 6.1).

3.2 Definition of the scalar seismic moment

Although the decomposition into M_{ISO}, M_{DC} and M_{CLVD} using base tensors (5) is quite common and is used by many authors, the definition of scale factors C_{ISO}, C_{DC} and C_{CLVD} in Eq. (9) is more ambiguous because of the variability of the definitions of scalar seismic moment M. In the above approach, M is defined by Eq. (10) as the sum of spectral norms of the individual components of moment tensor **M**. The same value of M is produced by the norm proposed by Bowers and Hudson (1999)

$$M = ||\mathbf{M}_{ISO}|| + ||\mathbf{M}_{DEV}||, \quad (13)$$

where $||\mathbf{M}_{ISO}||$ and $||\mathbf{M}_{DEV}||$ are the spectral norms of the isotropic and deviatoric parts of moment tensor **M**, respectively.

Note that the simplest option when M is calculated as the spectral norm of complete moment tensor **M**:

$$M = \max(|M_1|, |M_2|, |M_3|) \tag{14}$$

cannot be applied in Eq. (9) because it leads to the violation of Eq. (11) if C_{ISO} and C_{CLVD} are of opposite signs. For example, Vavryčuk (2001, 2005) uses the spectral norm of **M** defined in Eq. (14) for calculating C_{ISO}, but factors C_{CLVD} and C_{DC} must then be scaled by another constant to satisfy Eq. (11):

$$C_{ISO} = \frac{M_{ISO}}{M}, C_{CLVD} = \frac{M_{CLVD}}{\overline{M}}, C_{DC} = \frac{M_{DC}}{\overline{M}}, \tag{15}$$

where

$$\overline{M} = \frac{|M_{CLVD}| + M_{DC}}{1 - |M_{ISO}| \Big/ M}. \tag{16}$$

If C_{ISO} and C_{CLVD} are of the same signs, Eqs. (15–16) yield the same scale factors C_{ISO}, C_{DC} and C_{CLVD} as when applied norms defined in Eq. (10) or Eq. (13).

Nevertheless, a consistent scaling of the ISO, DC and CLVD components by the spectral norm of **M** can still find applications, for example, when constructing the Hudson skewed diamond source-type plot (see Section 6.1).

On the contrary, Silver and Jordan (1982) prefer defining M in a quite different way—using the Euclidean (Frobenius) norm:

$$M = \sqrt{\frac{1}{2}\left(M_1^2 + M_2^2 + M_3^2\right)}, \tag{17}$$

where factor 1/2 is used for consistency with the standard definition of the scalar seismic moment (Aki and Richards 2002, their Eq. 3.16). For the pure DC source, norms (10) and (17) yield the same moment M; hence, they apparently seem to be equally suitable for being used in the moment tensor decomposition. However, using the Euclidean norm for M in the above decomposition is mathematically inconvenient and introduces difficulties because it is inconsistent with the definition of the norms of the base tensors (5). A mathematically consistent decomposition based on exclusively using the Euclidean norm will be described in Section 5.2.

3.3 Physical properties of the decomposition

The decomposition of the moment tensor is performed in order to physically interpret a set of nine dipole forces representing a general point seismic source and to easily identify some basic types of the source in isotropic media:

- The explosion/implosion is an isotropic source, and thus it is characterized by $C_{ISO}=\pm 1$ and by zero C_{CLVD} and C_{DC}.
- Shear faulting is represented by the double-couple force and characterized by $C_{DC}=1$ and by zero C_{ISO} and C_{CLVD}.
- Pure tensile or compressive faulting is free of shearing and thus characterized by zero C_{DC}. However, the non-DC components contain both ISO and CLVD. The ISO and CLVD components are of the same sign: they are positive for tensile faulting but negative for compressive faulting (Vavryčuk 2001, 2011).
- The shear-tensile (dislocation) source defined as the source, which combines both shear and tensile faulting (Vavryčuk 2001, 2011), is characterized by non-zero ISO, DC and CLVD components. The positive values of C_{ISO} and C_{CLVD} correspond to tensile mechanisms when the fault is opening during rupturing. The negative values of C_{ISO} and C_{CLVD} correspond to compressive mechanisms when the fault is closing during rupturing. The ratio between the non-DC and DC components defines the angle between the slip and the fault.
- Shear faulting on a non-planar fault is characterized generally by a non-zero C_{DC} and C_{CLVD}. The C_{ISO} is zero because no volumetric changes are associated with this type of source.

3.4 Graphical representation of the decomposition

The moment tensor decomposition can be displayed and easily interpreted using a diamond source-type plot (Fig. 1). The plot shows the position of the source in the CLVD–ISO coordinate system in which the DC component is represented by the colour intensity. A source with pure or predominant shear faulting is located at the origin of coordinates or close to it. Explosions and implosions are located at the top and bottom vertex of the diamond, respectively. Pure tensile and compressive cracks are plotted at the margins of the diamond. Points along the CLVD axis correspond to faulting on

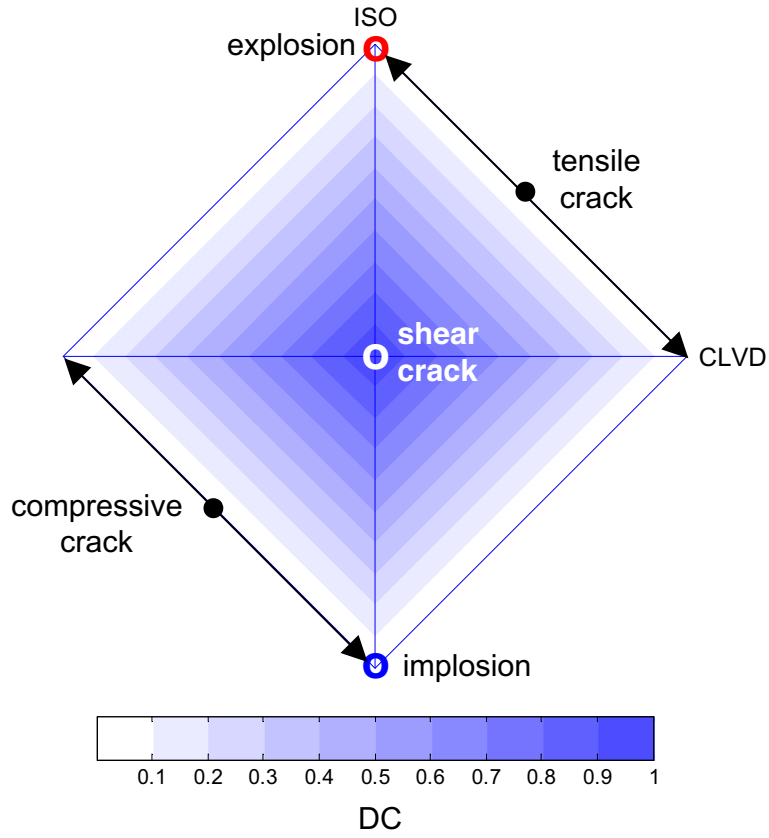

Fig. 1 The diamond CLVD–ISO plot with the positions of the basic types of seismic sources. The *arrows* indicate the range of the possible positions of moment tensors for pure tensile or compressive cracks

non-planar faults and points in the first and third quadrants of the diamond correspond to shear-tensile sources.

For pure tensile and shear-tensile sources, the ISO/CLVD ratio depends on the elastic properties of the medium surrounding the source (Vavryčuk 2001, 2011). In isotropic media, this ratio is:

$$\frac{C_{\mathrm{ISO}}}{C_{\mathrm{CLVD}}} = \frac{3}{4}\left(\frac{v_P}{v_S}\right)^2 - 1. \tag{18}$$

Hence, the point representing pure tensile faulting in Fig. 1 (black dot) can be close to $C_{\mathrm{ISO}}=1$ (corresponding to an explosion) for high values of v_P/v_S but also close to $C_{\mathrm{CLVD}}=1$ for low values of v_P/v_S. The limiting cases are:

$$\frac{v_P}{v_S} \to \infty \quad \text{and} \quad \frac{v_P}{v_S} = \frac{2}{\sqrt{3}}, \tag{19}$$

describing fluids and the lower limit of stable solids ($\lambda = -2/3\,\mu$), respectively. Similar conclusions can be drawn for pure compressive faulting.

Note that the above-mentioned basic types of sources cannot be located in the second or fourth quadrants of the diamond source-type plot. Moment tensors in this area may indicate errors of the moment tensor inversion due to noise in data, limited data coverage, an inaccurate velocity model, a more complicated source model or faulting in anisotropic media.

As mentioned earlier, in isotropic media, $C_{\mathrm{ISO}}=\pm 1$ and $C_{\mathrm{DC}}=1$ correspond to an explosion/implosion and to shear faulting, respectively. Their physical meaning is thus straightforward. However, the moment tensor with $C_{\mathrm{CLVD}}=\pm 1$ does not correspond to any simple physical seismic source, and the presence of CLVD in moment tensors often causes confusions and poses questions as to whether it is necessary to introduce the CLVD. The decomposition described earlier indicates that the CLVD component is required to render the decomposition mathematically complete, and the CLVD cannot thus be avoided. Although it has no simple physical meaning itself, it can be interpreted physically in combination with the ISO component as a product of tensile faulting. In the case of a pure tensile crack, the major dipole of the CLVD component is aligned with the normal to the crack surface, and the volume change

associated with the opening crack is described by the ISO component. However, in the case of shear-tensile faulting, the CLVD major dipole need not be normal to the fault, and also the orientation of DC component is not simply related to the fault plane.

4 Source tensor decomposition

A simple classification of sources based on the moment tensor decomposition is possible in isotropic media only. In anisotropic media, the problem is more complicated. The moment tensor of an explosive/implosive source is characterized by $C_{\mathrm{ISO}}=\pm 1$ in isotropic as well as anisotropic media, but the moment tensor of an earthquake source is affected not only by the geometry of faulting but also by the elastic properties of the material in the focal zone. Depending on these properties, the moment tensors can take a general form with non-zero ISO, DC and CLVD components even for simple shear faulting on a planar fault (Vavryčuk 2005). For this reason, physical interpretations of earthquake sources (i.e. shear-tensile dislocation sources) in anisotropic media should be based on the decomposition of the source tensor, which is directly related to the geometry of faulting.

The source tensor **D** of a dislocation source (also called the potency tensor, see Ben-Zion 2001, 2003; Ampuero and Dahlen 2005) is a symmetric dyadic tensor defined as (Ben-Zion 2003; Vavryčuk 2005):

$$D_{kl} = \frac{uS}{2}(s_k n_l + s_l n_k), \tag{20}$$

where unit vectors **n** and **s** denote the fault normal and the direction of the slip vector, respectively, u is the slip and S is the fault size. In anisotropic media, the relation between the source and moment tensors reads (Vavryčuk 2005, his Eq. 4):

$$M_{ij} = c_{ijkl} D_{kl}, \tag{21}$$

and in isotropic media

$$M_{ij} = \lambda D_{kk}\delta_{ij} + 2\mu D_{ij}, \tag{22}$$

where c_{ijkl} is the tensor of elastic parameters, and λ and μ are the Lamé's parameters. While the moment and source tensors diagonalize in anisotropic media in different systems of eigenvectors and thus their relation is complicated, the eigenvectors of the moment and source tensors are the same in isotropic media and their decomposition according to the formulas in Section 3.1 yields similar results.

The properties of the moment and source tensor decompositions for shear and tensile sources in isotropic and anisotropic media are illustrated in Figs. 2 and 3. Figure 2 shows the source-type plots for shear-tensile sources with a variable slope angle (i.e. the deviation of the slip vector from the fault, see Vavryčuk 2011) situated in an isotropic medium. The plot shows that the scale factors of the ISO and CLVD components are linearly dependent for both moment and source tensors. For the moment tensors, the line direction depends on the v_P/v_S ratio (Fig. 2a). For the source tensors, the line is independent of the properties of the elastic medium and the $C_{\mathrm{ISO}}/C_{\mathrm{CLVD}}$ ratio is always 1/2 (see Fig. 2b and Appendix B). This property is preserved even for anisotropic media. On the contrary, the moment tensors can behave in a more complicated way in anisotropic media. Figure 3 shows the ISO and CLVD components of the moment tensors of shear (Fig. 3a) or shear-tensile (Fig. 3b) faulting in the Bazhenov shale (Vernik and Liu 1997). This complicated behaviour prevents a straightforward interpretation of moment tensors in terms of the physical faulting parameters. Therefore, first the source tensors must be calculated from moment tensors and then interpreted. If the elastic properties of the medium in the focal zone needed for calculating the source tensors are not known, they can be inverted from the non-DC components of the moment tensors (Vavryčuk 2004, 2011; Vavryčuk et al. 2008). Note that the retrieved medium parameters do not refer to local material properties of the fault but to the medium surrounding the fault and depend on the wavelength of the analysed radiated waves.

5 Alternative decompositions

Obviously, moment and source tensor decompositions can be proposed in many alternative ways. They differ in the definition and scaling of the base tensors. Here we list several alternative approaches and mention their pros and cons.

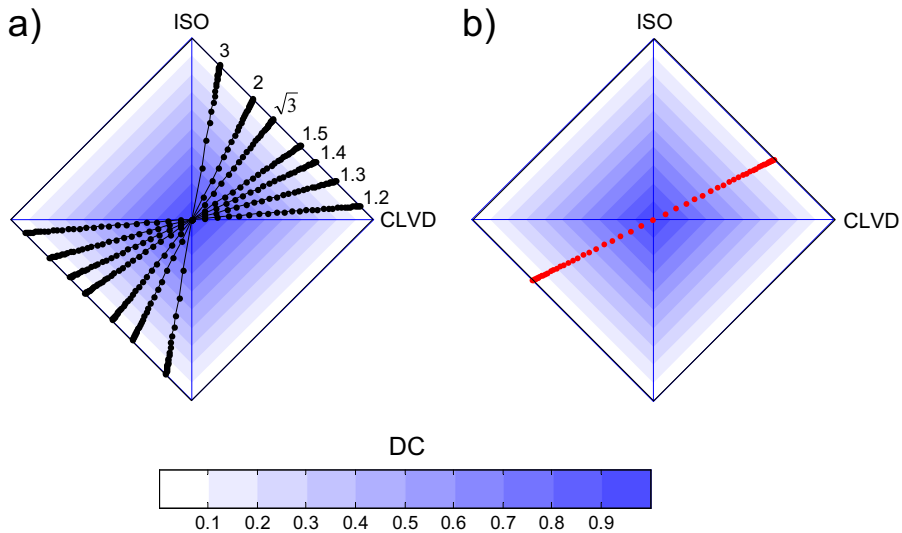

Fig. 2 The source-type plots for the moment (**a**) and source (**b**) tensors for shear-tensile faulting in an isotropic medium characterized by various values of the v_P/v_S ratio (the values are indicated in the plot). *Red dots* source tensors, *black dots* moment tensors. The *dots* correspond to the sources with a specific value of the slope angle (i.e. the deviation of the slip vector from the fault). The slope angle ranges from −90° (pure compressive crack) to 90° (pure tensile crack) in steps of 3°

5.1 A new simplified moment tensor decomposition

The properties of the decomposition described by Eqs. (6–10) depend on the scaling of base tensors which control the fractional amounts of the ISO, DC and CLVD components present in a general moment tensor. If the normalization is properly modified, the final moment decomposition formulas can be

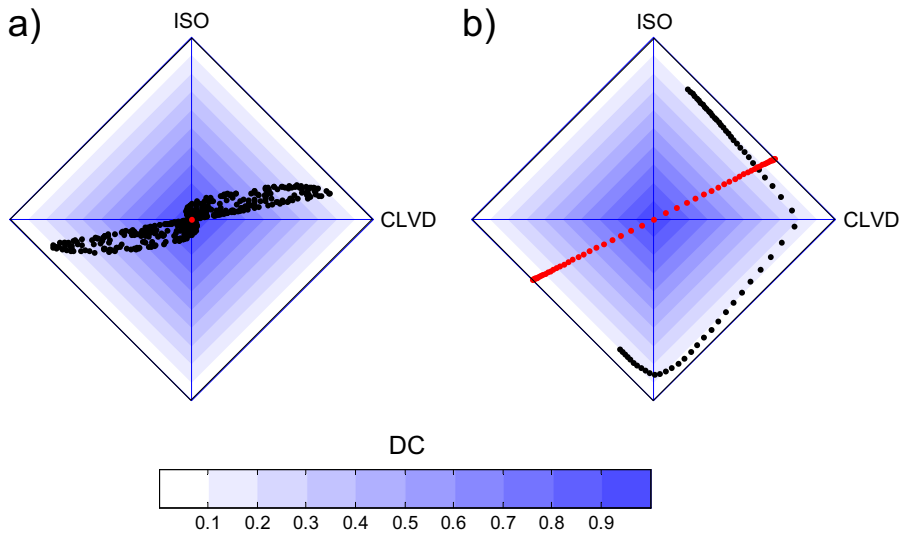

Fig. 3 The source-type plots for pure shear (**a**) and shear-tensile (**b**) faulting in an anisotropic medium. The *black dots* in **a** correspond to 500 moment tensors of shear sources with randomly oriented faults and slips. The *black dots* in **b** correspond to the moment tensors of shear-tensile sources with strike=0°, dip=20° and rake=−90° (normal faulting). The slope angle ranges from −90° (pure compressive crack) to 90 ° (pure tensile crack) in steps of 3°. The *red dots* in **a** and **b** show the corresponding source tensors. The medium is transversely isotropic with the following elastic parameters (in 10^9 kg m^{-1} s^{-2}): c_{11}=58.81, c_{33}=27.23, c_{44}=13.23, c_{66}=23.54 and c_{13}=23.64. The medium density is 2,500 kg/m^3. The parameters are taken from Vernik and Liu (1997) and describe the Bazhenov shale (depth of 12.507 ft)

simplified. For example, if we adopt base tensors as follows:

$$\mathbf{E}_{\mathrm{ISO}} = \frac{2}{3}\begin{bmatrix} 1 & 0 & 0 \\ 0 & 1 & 0 \\ 0 & 0 & 1 \end{bmatrix}, \tag{23}$$

$$\mathbf{E}_{\mathrm{DC}} = \begin{bmatrix} 1 & 0 & 0 \\ 0 & 0 & 0 \\ 0 & 0 & -1 \end{bmatrix},$$

$$\mathbf{E}^{+}_{\mathrm{CLVD}} = \frac{2}{3}\begin{bmatrix} 2 & 0 & 0 \\ 0 & -1 & 0 \\ 0 & 0 & -1 \end{bmatrix},$$

$$\mathbf{E}^{-}_{\mathrm{CLVD}} = \frac{2}{3}\begin{bmatrix} 1 & 0 & 0 \\ 0 & 1 & 0 \\ 0 & 0 & -2 \end{bmatrix},$$

the relative ISO, DC and CLVD scale factors read

$$\begin{bmatrix} C_{\mathrm{ISO}} \\ C_{\mathrm{CLVD}} \\ C_{\mathrm{DC}} \end{bmatrix} = \frac{1}{2M}\begin{bmatrix} M_1 + M_2 + M_3 \\ M_1 + M_3 - 2M_2 \\ M_1 - M_3 - |M_1 + M_3 - 2M_2| \end{bmatrix}, \tag{24}$$

where

$$M = \frac{1}{2}\left(|M_1 + M_2 + M_3| + M_1 - M_3\right), \tag{25}$$

and the ISO/CLVD ratio for shear-tensile faulting in isotropic media reads

$$\frac{C_{\mathrm{ISO}}}{C_{\mathrm{CLVD}}} = \frac{3}{8}\left(\frac{v_P}{v_S}\right)^2 - \frac{1}{2}. \tag{26}$$

The other properties of the decomposition: explosion/implosion producing $C_{ISO}=\pm 1$, shear faulting being characterized by $C_{DC}=1$, and pure tensile faulting producing no DC, remain unchanged (see Fig. 4). The formula for **M** is identical with Eq. (12,) but the scalar seismic moment M is now defined by Eq. (25). Note that if we adopt Eq. (25) as the formula for the tensor norm, the norms of the base tensors in Eq. (23) are equal to 1 similarly as for the standard moment tensor decomposition. Also, the scalar seismic moment for the pure DC source coincides with the standard definition. The disadvantage of this decomposition, however, is that the magnitude of dipole forces is different for different elementary source tensors, so that the physical insight into the decomposition is not as straightforward as for the standard decomposition.

5.2 Euclidean moment tensor decomposition

The decomposition into the ISO, DC and CLVD components can also be performed by normalizing base tensors $\mathbf{E}_{\mathrm{ISO}}$, $\mathbf{E}_{\mathrm{DC}}$ and $\mathbf{E}_{\mathrm{CLVD}}$ using the Euclidean (Frobenius) norm:

$$\|\mathbf{E}\| = \sqrt{\frac{1}{2}E_{kl}E_{kl}} = 1, \tag{27}$$

where the summation over repeated indices is applied. The coefficient 1/2 is used in Eq. (27) to produce the scalar seismic moment consistent with the standard definition for the pure DC source. According to Chapman and Leaney (2012), the base tensors are defined as:

$$\mathbf{E}^{*}_{\mathrm{ISO}} = \sqrt{\frac{2}{3}}\begin{bmatrix} 1 & 0 & 0 \\ 0 & 1 & 0 \\ 0 & 0 & 1 \end{bmatrix}, \tag{28}$$

$$\mathbf{E}^{*}_{\mathrm{DC}} = \begin{bmatrix} 1 & 0 & 0 \\ 0 & 0 & 0 \\ 0 & 0 & -1 \end{bmatrix},$$

$$\mathbf{E}^{*}_{\mathrm{CLVD}} = \frac{1}{\sqrt{3}}\begin{bmatrix} 1 & 0 & 0 \\ 0 & -2 & 0 \\ 0 & 0 & 1 \end{bmatrix},$$

where the asterisk is used to distinguish between the base tensors defined in Eq. (28) and in Eq. (5) used in the standard decomposition. Both sets of base tensors differ in two basic aspects: in the normalization and in the definition of the CLVD tensor. The CLVD tensor in Eq. (28) is rotated to lie along the N axis but not along the P or T axes as in Eq. (5). The modification of the CLVD is needed for the base tensors to form an orthogonal system:

$$\begin{aligned}\left(\mathbf{E}^{*}_{\mathrm{ISO}}\right)_{kl}\left(\mathbf{E}^{*}_{\mathrm{DC}}\right)_{kl} &= \left(\mathbf{E}^{*}_{\mathrm{ISO}}\right)_{kl}\left(\mathbf{E}^{*}_{\mathrm{CLVD}}\right)_{kl} \\ &= \left(\mathbf{E}^{*}_{\mathrm{DC}}\right)_{kl}\left(\mathbf{E}^{*}_{\mathrm{CLVD}}\right)_{kl} = 0,\end{aligned} \tag{29}$$

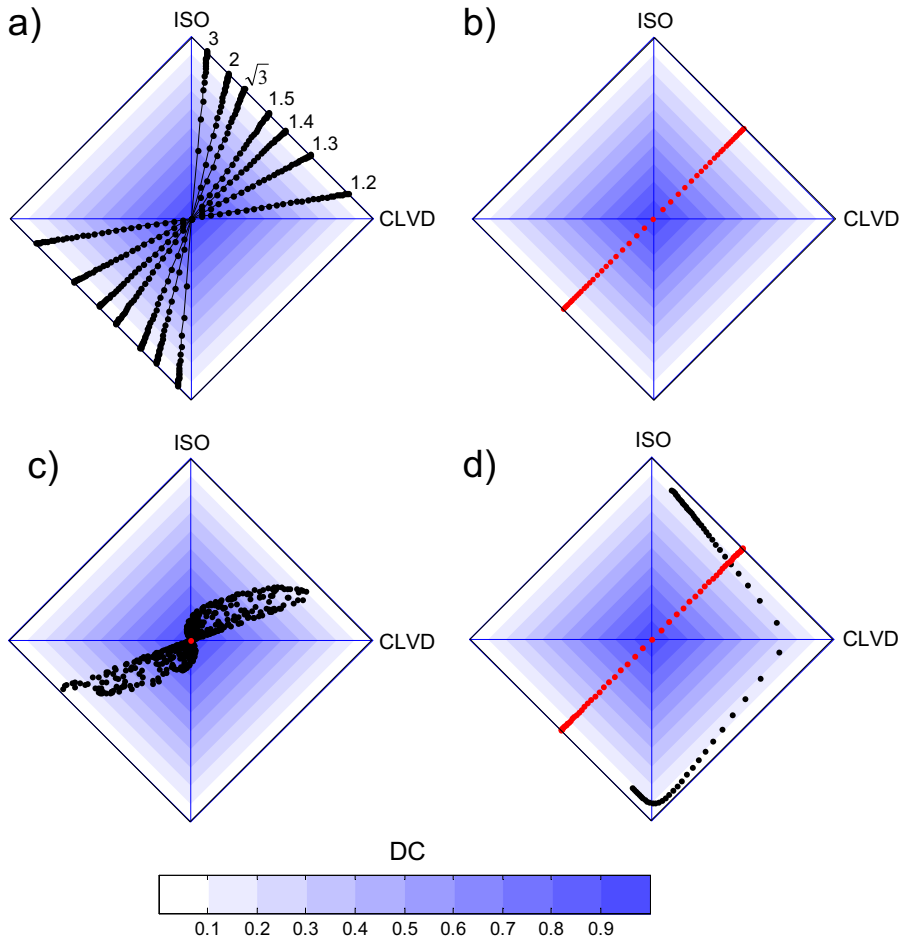

Fig. 4 The source-type plots for shear-tensile faulting in isotropic media (**a**, **b**) and for pure shear (**c**) and shear-tensile (**d**) faulting in anisotropic media for the simplified decomposition (see Section 5.1). The *dots* in **a** and **b** correspond to the shear-tensile sources with the slope angle ranging from −90° (pure compressive crack) to 90° (pure tensile crack) in steps of 3°. The *black dots* in **a** correspond to the moment tensors; the *red dots* in **b** correspond to the source tensors. The *black dots* in **c** correspond to 500 moment tensors of shear sources with randomly oriented faults and slips. The *black dots* in **d** correspond to the moment tensors of shear-tensile sources with strike=0°, dip=20° and rake=−90° (normal faulting). The *red dots* in **c** and **d** show the corresponding source tensors. The medium in **c** and **d** is transversely isotropic (see the caption of Fig. 3)

and thus applying the Euclidean norm to be meaningful. The Euclidean norm produces M^*_{ISO}, M^*_{CLVD} and M^*_{DC} as follows:

$$M^*_{\mathrm{ISO}} = \frac{1}{\sqrt{6}}(M_1 + M_2 + M_3), \tag{30}$$

$$M^*_{\mathrm{CLVD}} = \frac{1}{2\sqrt{3}}(M_1 + M_3 - 2M_2), \tag{31}$$

$$M^*_{\mathrm{DC}} = \frac{1}{2}(M_1 - M_3). \tag{32}$$

Scalar seismic moment M^* reads:

$$M^* = \sqrt{\frac{1}{2}\left(M_1^2 + M_2^2 + M_3^2\right)} = \sqrt{\frac{1}{2}\left(M_{\mathrm{ISO}}^2 + M_{\mathrm{CLVD}}^2 + M_{\mathrm{DC}}^2\right)}. \tag{33}$$

The scale factors C^*_{ISO}, C^*_{CLVD} and C^*_{DC} are defined as:

$$\begin{bmatrix} C^*_{\mathrm{ISO}} \\ C^*_{\mathrm{CLVD}} \\ C^*_{\mathrm{DC}} \end{bmatrix} = \frac{1}{\left(M^*\right)^2} \begin{bmatrix} \mathrm{sign}\left(M^*_{\mathrm{ISO}}\right) & \left(M^*_{\mathrm{ISO}}\right)^2 \\ \mathrm{sign}\left(M^*_{\mathrm{CLVD}}\right) & \left(M^*_{\mathrm{CLVD}}\right)^2 \\ & \left(M^*_{\mathrm{DC}}\right)^2 \end{bmatrix}, \tag{34}$$

in order to satisfy

$$\left|C^*_{\mathrm{ISO}}\right| + \left|C^*_{\mathrm{CLVD}}\right| + C^*_{\mathrm{DC}} = 1, \tag{35}$$

similarly as for the standard decomposition (11).

Let us briefly discuss the mathematical and physical consequences of the decomposition based on using the Euclidean norm. Despite the attractive mathematical properties of the Euclidean norm, applying this norm to the moment tensor decomposition leads to consequences which are rather undesirable and might disqualify this decomposition from being routinely employed in seismological practice. The reasons are as follows:

1. As mentioned earlier, the major dipole of the CLVD base tensor lies along the N axis in order to satisfy the orthogonality condition (29). However, this condition applies to the full 3-D space but not to the source-type space. As a consequence, the newly defined CLVD base tensor does not satisfy the ordering of eigenvalues prescribed by Eq. (2) and does not lie in the source-type space. If we decompose any general moment tensor using base tensors $\mathbf{E}^*_{\mathrm{ISO}}$, $\mathbf{E}^*_{\mathrm{DC}}$ and $\mathbf{E}^*_{\mathrm{CLVD}}$:

$$\begin{aligned} \mathbf{M} &= \mathbf{M}^*_{\mathrm{ISO}} + \mathbf{M}^*_{\mathrm{DC}} + \mathbf{M}^*_{\mathrm{CLVD}} \\ &= M^*_{ISO}\ \mathbf{E}^*_{\mathrm{ISO}} + M^*_{\mathrm{DC}}\ \mathbf{E}^*_{\mathrm{DC}} + M^*_{\mathrm{CLVD}}\ \mathbf{E}^*_{\mathrm{CLVD}}, \end{aligned} \tag{36}$$

we find that the last term on the rhs $\mathbf{M}^*_{\mathrm{CLVD}}$ is 'unstable' because it lies outside the source-type space. If $\mathbf{M}^*_{\mathrm{CLVD}}$ is further decomposed as an individual tensor, its eigenvalues must be reordered according to Eq. (2), and $\mathbf{M}^*_{\mathrm{CLVD}}$ subsequently splits into another non-zero $\mathbf{M}^*_{\mathrm{DC}}$ and $\mathbf{M}^*_{\mathrm{CLVD}}$. This property violates the basic condition imposed on the base vectors (tensors) in linear vector spaces.

2. As a consequence of the previous point, the relative scale factor C^*_{CLVD} can never attain the value of ±1 even for any of the following pure CLVD moment tensors:

$$\mathbf{M}_1 = \frac{1}{2}\begin{bmatrix} 2 & 0 & 0 \\ 0 & -1 & 0 \\ 0 & 0 & -1 \end{bmatrix}, \tag{37}$$

$$\mathbf{M}_2 = \frac{1}{2}\begin{bmatrix} -1 & 0 & 0 \\ 0 & 2 & 0 \\ 0 & 0 & -1 \end{bmatrix},$$

$$\mathbf{M}_3 = \frac{1}{2}\begin{bmatrix} -1 & 0 & 0 \\ 0 & -1 & 0 \\ 0 & 0 & 2 \end{bmatrix},$$

because, first, their eigenvalues have to be ordered, and after that they can be decomposed. Their scale factors are C^*_{CLVD}=1/4 and C^*_{DC}=3/4.

3. The spectral norm (10) used in the standard decomposition keeps the magnitude of the largest eigenvalue equal to 1. This physically means that the predominant linear vector dipoles in all base tensors have the same magnitude. Hence, the scale factors C_{ISO}, C_{CLVD} and C_{DC} measure directly the relative magnitudes of the dipole forces in the source. For example, if the moment tensor is composed of the following $\mathbf{M}_{\mathrm{ISO}}$ and $\mathbf{M}_{\mathrm{DC}}$ tensors:

$$\mathbf{M}_{\mathrm{ISO}} = \begin{bmatrix} 1 & 0 & 0 \\ 0 & 1 & 0 \\ 0 & 0 & 1 \end{bmatrix}, \tag{38}$$

$$\mathbf{M}_{\mathrm{DC}} = 2\begin{bmatrix} 1 & 0 & 0 \\ 0 & 0 & 0 \\ 0 & 0 & -1 \end{bmatrix},$$

then C_{DC} is obviously twice larger than C_{ISO}, C_{DC}=2/3 and C_{ISO}=1/3. However, applying the Euclidean norm leads to C^*_{DC} larger than C^*_{ISO} by a factor of 8/3: C^*_{DC}=8/11 and C^*_{SO}=3/11. This might complicate a physical insight into the decomposition.

4. Defining the major dipole of the CLVD along the N axis causes the moment tensor for pure tensile (or compressive) faulting to contain a non-zero DC component (see Chapman and Leaney 2012, their Eq. B12a). If the v_P/v_S ratio is 1.73, the DC percentage is 18 %. This property is awkward because it violates the basic requirement imposed on moment tensor decompositions that the presence of shear faulting is measured by the amount of DC. Consequently, we expect pure tensile faulting to generate no DC since it is free of shearing. Obviously, a decomposition which does not respect

such conditions complicates the physical interpretations of a seismic source.

5.3 Crack-plus-double-couple model

Minson et al. (2007) analysed non-double-couple mechanisms of volcanic earthquakes on Miyakejima, Japan, and introduced a model which combines shear faulting with crack opening, calling this model the 'crack-plus-double-couple' (CDC) model. The authors further developed a non-linear scheme for directly inverting for the parameters of this source model from seismic observations. Since the model does not describe all source types, only two eigenvalues of moment tensor **M** are independent. For this reason, the authors do not distinguish between ISO and CLVD components and calculate just the percentages of the DC and non-DC components using the following formula:

$$C_{\text{non-DC}} = \frac{M_C}{M_0 + M_C} 100\%, \tag{39}$$

where M_0 and M_C are the scalar moments of the shear and tensile cracks defined as

$$\mathbf{M}_{\text{DC}} = M_0 \begin{bmatrix} 1 & 0 & 0 \\ 0 & 0 & 0 \\ 0 & 0 & -1 \end{bmatrix}, \tag{40}$$

$$\mathbf{M}_{\text{crack}} = M_C \begin{bmatrix} 1 & 0 & 0 \\ 0 & 1 & 0 \\ 0 & 0 & \dfrac{\lambda + 2\mu}{\lambda} \end{bmatrix},$$

where λ and μ are the Lamé coefficients of the medium in the focal zone.

If we compare the CDC model with the other previously developed models, we find that the CDC model is, in fact, similar with the tectonic model of Dufumier and Rivera (1997) or with the shear-tensile model of Vavryčuk (2001, 2011). Hence, the CDC, tectonic and shear-tensile models can all be treated in a standard way using the decomposition of the moment and source tensors into the ISO, DC and CLVD components as described in Sections 3 and 4. The standard decomposition has particularly two basic advantages compared to the CDC model. Firstly, it is not necessary to assume a priori that the source is described by the shear-tensile model. This type of a source is recognized by the linear dependence between the ISO and CLVD scale factors when analysing moment tensors of the shear-tensile sources in the same (isotropic) focal area. Secondly, the CDC decomposition cannot be applied without knowledge of the v_P/v_S ratio (or equivalently of the Poison ratio) in the focal area. The standard decomposition does not require knowing this value. It is even possible to determine this value from the ISO/CLVD ratio (see Eq. (18)).

However, the idea of inverting for the parameters of the shear-tensile source model directly from seismic observations in order to stabilize the inversion is original and valuable since it was applied later also by other authors (Vavryčuk 2011; Stierle et al. 2014a, b).

5.4 Other decompositions

When seismologists started to analyse general moment tensors, many alternative approaches of decomposing the moment tensors into 'elementary' force systems were proposed. Ambiguities mostly appeared in decomposing the deviatoric part of the moment tensor. It was decomposed, for example, into three DCs, into major and minor DC, into two DCs with the same *T* axes or into the DC and variously oriented CLVDs (for a review, see Julian et al. 1998). Over time, these decompositions were mostly abandoned because they proved unsuitable for mathematical or physical reasons. Let us summarize a few of the main reasons:

1. The source-type space is a wedge in full 3-D space. Therefore, decomposing the moment tensor into ISO and three DCs is an unnecessary overparameterization with no clear advantage.
2. Except for the moment tensor decompositions described in Sections 3.1 and 5.1, no other approach offers decomposing the moment tensors into elementary force systems which all lie in the source-type space. If any of the elementary force systems is outside the source-type space, the decomposition introduces mathematical difficulties because these force systems cannot be considered as the base vectors in this space. This means that the individual components of the moment tensor violate the ordering condition (2), and when further analysed, they split into other components. Mathematically, this means that the decomposition is not a linear transformation within the source-type space.
3. The decompositions fail to be sufficiently general for physical interpretations. For example, the decomposition of the deviatoric part of the moment tensor into a

major DC and some minor residual component is justified and appropriate if the analysed moment tensor describes shear faulting on a planar fault in isotropic media. The major DC would correspond to the true shear faulting, and the residual component would represent errors due to the inversion or due to data limitations. However, if the source represents shear-tensile faulting or pure tensile faulting, this decomposition is not helping in the interpretations because it cannot be used for identifying this type of a source. This applies also to the other mentioned decompositions.

6 Alternative source-type plots

All moment tensors fill a source-type space which is a wedge in the full 3-D space. The magnitude of the vector in this space is the scalar moment, and its direction defines the type of the source. In order to identify the type of the source visually, it is convenient to plot all unit vectors of the source-type space in a 2-D figure using some projection. We distinguish three basic kinds of the source-type plots depending on the norm applied to the source-type space (see Fig. 5):

1. Diamond CLVD-ISO plot. If the norm is defined as the sum of the spectral norms of the individual tensor components using Eq. (10), we map points which cover partly the surface of two pyramids with a common hexagonal base (see Section 3.4).
2. Hudson's skewed diamond plot. If the spectral norm (Eq. 14) is used, we map points which cover partly the surface of a cube (see Section 6.1).
3. Riedesel–Jordan lune plot. If the Euclidean norm (Eq. 17) is used, we map points which cover partly the surface of a sphere (see Section 6.2).

If we assume a random distribution of moment tensors in the source-type space, the three above-mentioned surfaces of unit distance are covered by the moment tensors uniformly. The projections of these surfaces into 2-D plots are chosen to conserve this property.

6.1 Hudson's skewed diamond plot

Hudson et al. (1989) introduced two source-type plots: a diamond τ–k plot and a skewed diamond u–v plot. The τ–k plot is the diamond CLVD–ISO plot described in Section 3.4 but with the opposite direction of the CLVD axis. The skewed diamond plot is introduced in order to conserve the uniform probability of moment tensor eigenvalues normalized by spectral norm (14). If we assume that the eigenvalues can attain values between −1 and +1 and satisfy the ordering condition (2), all points then fill a volume forming a wedge inside a cube (see Tape and Tape 2012b, their Fig. 5). The unit vectors fill two half-faces on this cube (see Fig. 6a, b). In the upper half-face (yellow colour), the normalized eigenvalue $\overline{M}_1$ equals 1, while in the lower half-face (red colour), the normalized eigenvalue $\overline{M}_3$ equals −1. The dashed line in Fig. 6b shows the deviatoric sources:

$$\overline{M}_1 + \overline{M}_2 + \overline{M}_3 = 0. \tag{41}$$

The two half-faces in Fig. 6b are further skewed, the dashed line defining deviatoric sources (axis u) and the dotted line connecting the explosive and implosive sources (axis v) to be mutually perpendicular and of unit length. The moment tensor with eigenvalues M_1, M_2 and M_3 is projected into the u–v plot using the following simple equations:

$$u = -\frac{2}{3}\left(\overline{M}_1 + \overline{M}_3 - 2\overline{M}_2\right), \tag{42}$$

$$v = \frac{1}{3}\left(\overline{M}_1 + \overline{M}_2 + \overline{M}_3\right),$$

where

$$\overline{M}_i = \frac{M_i}{\max(|M_1|, |M_2|, |M_3|)}, \quad i = 1, 2, 3. \tag{43}$$

Equation (42) is similar to Eqs. (6–7) for the standard decomposition into the CLVD and ISO except for scaling. It is emphasized that the eigenvalues in Eq. (42) are normalized to their maximum absolute magnitude, hence $\overline{M}_1 = 1$ for the upper half-face (in yellow colour) and $\overline{M}_3 = -1$ for the lower half-face (in red colour). Equation (42) ensures that the skewed diamond u–v plot satisfies the requirement of the uniform probability distribution function (PDF) for sources with random eigenvalues because the coordinates u and v depend linearly on $\overline{M}_1$, $\overline{M}_2$ and $\overline{M}_3$. Note that in contrast to Hudson's original derivation which is rather complicated and treats the individual quadrants of the plot separately, the presented formula is simple and valid for all quadrants.

Figure 7 shows the mapping of a regular grid in C_{ISO} and C_{CLVD} calculated using Eqs. (6–10) into the

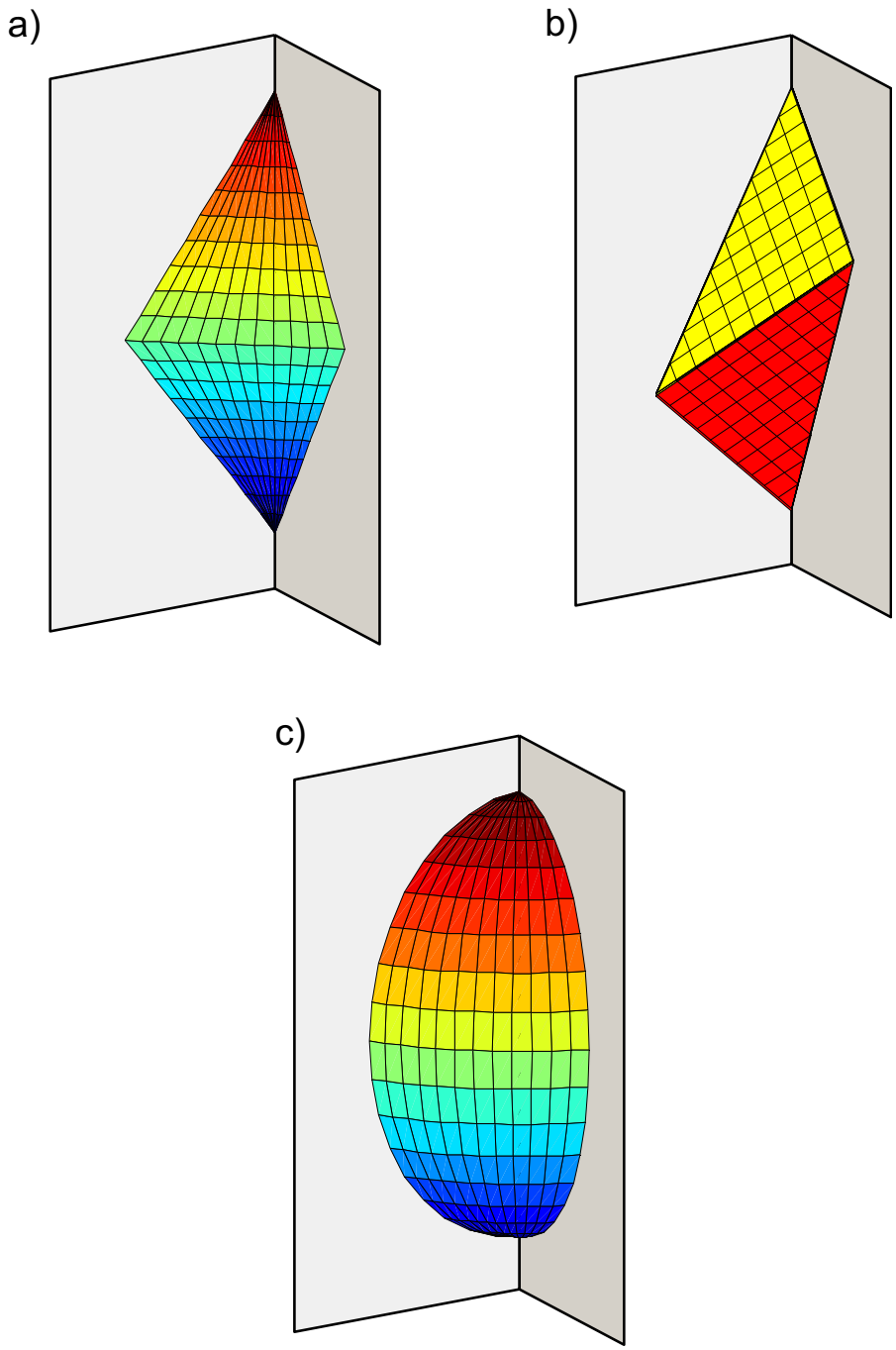

Fig. 5 Surfaces of unit vectors in the source-type space. The norm of moment tensor is defined as: **a** the sum of spectral norms of the base tensors (see Eq. (10)), **b** the spectral norm of moment tensor **M** (see Eq. (14)), and **c** the Euclidean norm of moment tensor **M** (see Eq. (17)). The colours are used for improving the 3-D visualization and have no physical meaning

diamond τ–k plot and into the skewed diamond u–v plot. Figure 7a proves that the τ–k plot is the CLVD–ISO plot with the reversed CLVD axis. Figure 7b shows that the CLVD–ISO grid is deformed in the first and third quadrants of the u–v plot. This is the reason why the sources satisfying the spectral norm (14) display a uniform PDF in Fig. 7d but a non-uniform PDF in Fig. 7c. In contrast, the sources satisfying the norm defined by

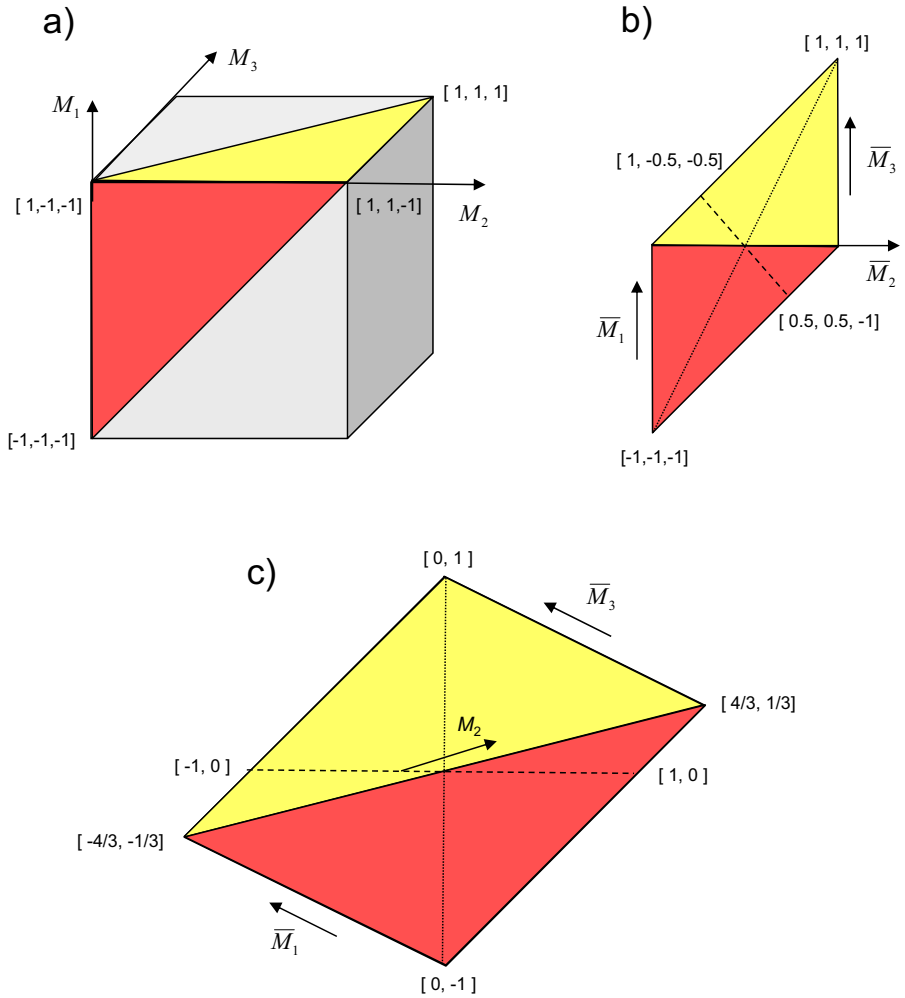

Fig. 6 A geometric interpretation of the Hudson's skewed diamond source-type plot. **a** The cube representing the volume of the moment tensor eigenvalues. **b** Half-faces corresponding to $M_1=1$ (in *yellow colour*) and $M_3=-1$ (in *red colour*). **c** The skewed diamond u–*v* plot. The *dashed line* defines the positions of the deviatoric sources; the *dotted line* is the ISO axis. The *arrows* in **b** and **c** show the orientation of axes of the individual eigenvalues

Eq. (10) display a uniform PDF in Fig. 7e but a non-uniform PDF in Fig. 7f. Hence, the norms must be applied consistently when generating and decomposing the moment tensors as well as when plotting the source types.

6.2 Riedesel–Jordan lune plot

A different approach is suggested by Riedesel and Jordan (1989) who introduced a compact plot displaying both the orientation and type of source on the focal sphere. The moment tensor is represented by a vector of the eigenvalues of **M** in a coordinate system formed by the eigenvectors of **M** (*P*, *T* and *N* axes):

$$\mathbf{m} = M_1\mathbf{e}_1 + M_2\mathbf{e}_2 + M_3\mathbf{e}_3. \quad (44)$$

The vector is normalized using the Euclidean norm and thus projected on a part of the sphere called the 'lune' (Tape and Tape 2012a) which covers one sixth of the whole sphere (see Fig. 5c). This surface is projected using a lower-hemisphere equal-area projection into a 2-D plot (see Fig. 8a). However, as pointed out by Chapman and Leaney (2012), this representation is not optimum for several reasons. Firstly, vectors characterizing positive and negative isotropic sources (explosion and implosion) are physically quite different, but they are displayed in the same area on the focal sphere in this projection. Secondly, the analysis of uncertainties of a

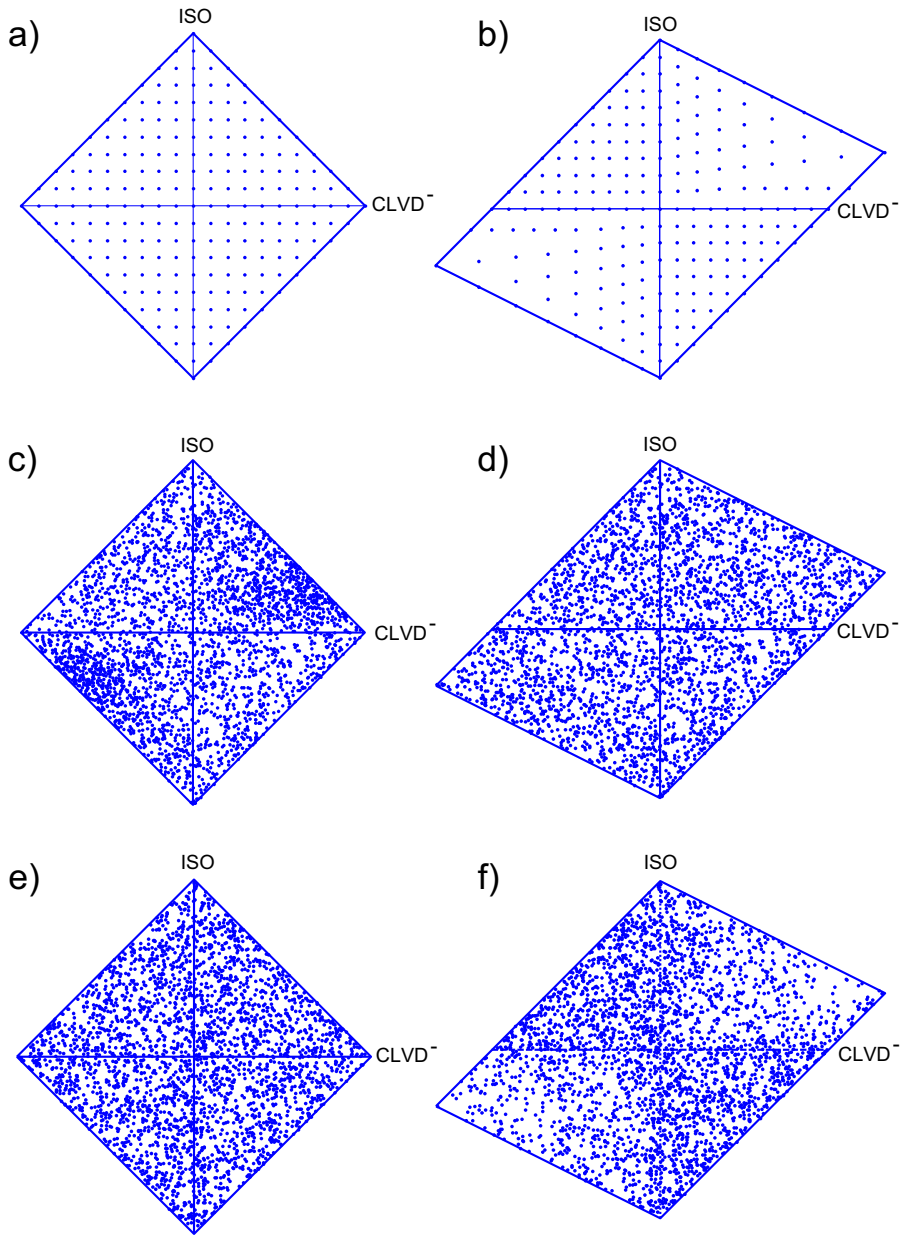

Fig. 7 The Hudson's diamond τ–k plot (**a**, **c**, **e**) and the skewed diamond u–v plot (**b**, **d**, **f**). The CLVD$^-$ means the reversed CLVD axis. The *dots* in **a** and **b** show a regular grid in C_{ISO} and C_{CLVD} from −1 to 1 with step of 0.1. The *dots* in **c** and **d** show 3,000 sources with randomly generated moment tensors satisfying the spectral norm (14). The *dots* in **e** and **f** show 3,000 sources with randomly generated moment tensors satisfying the norm (10). Plots **d** and **e** indicate that the distribution of sources is uniform if the moment tensors are generated and decomposed using the same norm. On the contrary, if the norms are mixed, the distribution of sources is non-uniform (see plots **c** and **f**)

moment tensor solution by plotting a cluster of vectors **m** includes both effects—uncertainties in the orientation as well as in the source type. This is fine if the moment tensor is non-degenerate. However, difficulties arise when the moment tensor is degenerate or nearly degenerate because small perturbations cause significant changes of eigenvectors.

The mentioned difficulties can be avoided by fixing the coordinate system. If we fix the coordinate axes in the form:

$$\mathbf{e}_1 = \left(\frac{1}{\sqrt{3}}, \frac{1}{\sqrt{6}}, \frac{1}{\sqrt{2}}\right)^T, \quad (45)$$

$$\mathbf{e}_2 = \left(\frac{1}{\sqrt{3}}, -\frac{2}{\sqrt{6}}, 0\right)^T,$$

$$\mathbf{e}_3 = \left(\frac{1}{\sqrt{3}}, \frac{1}{\sqrt{6}}, -\frac{1}{\sqrt{2}}\right)^T,$$

in the north-east-down coordinate system, we obtain the plot (Fig. 8b) suggested by Chapman and Leaney (2012) which resembles the CLVD–ISO diamond source-type plot (Fig. 1) but adapted to a spherical metric. The basic source types are characterized by the following unit vectors:

$$\mathbf{e}_{\mathrm{ISO}} = \frac{1}{\sqrt{3}}(\mathbf{e}_1 + \mathbf{e}_2 + \mathbf{e}_3) = (1,0,0)^T, \quad (46)$$

$$\mathbf{e}_{\mathrm{DC}} = \frac{1}{\sqrt{2}}(\mathbf{e}_1 - \mathbf{e}_3) = (0,0,1)^T, \quad (47)$$

$$\mathbf{e}_{\mathrm{CLVD}} = \sqrt{\frac{2}{3}}\left(\frac{1}{2}\mathbf{e}_1 - \mathbf{e}_2 + \frac{1}{2}\mathbf{e}_3\right) = (0,1,0)^T, \quad (48)$$

$$\mathbf{e}^+_{\mathrm{CLVD}} = \sqrt{\frac{2}{3}}\left(\mathbf{e}_1 - \frac{1}{2}\mathbf{e}_2 - \frac{1}{2}\mathbf{e}_3\right) = \left(0, \frac{1}{2}, \frac{\sqrt{3}}{2}\right)^T, \quad (49)$$

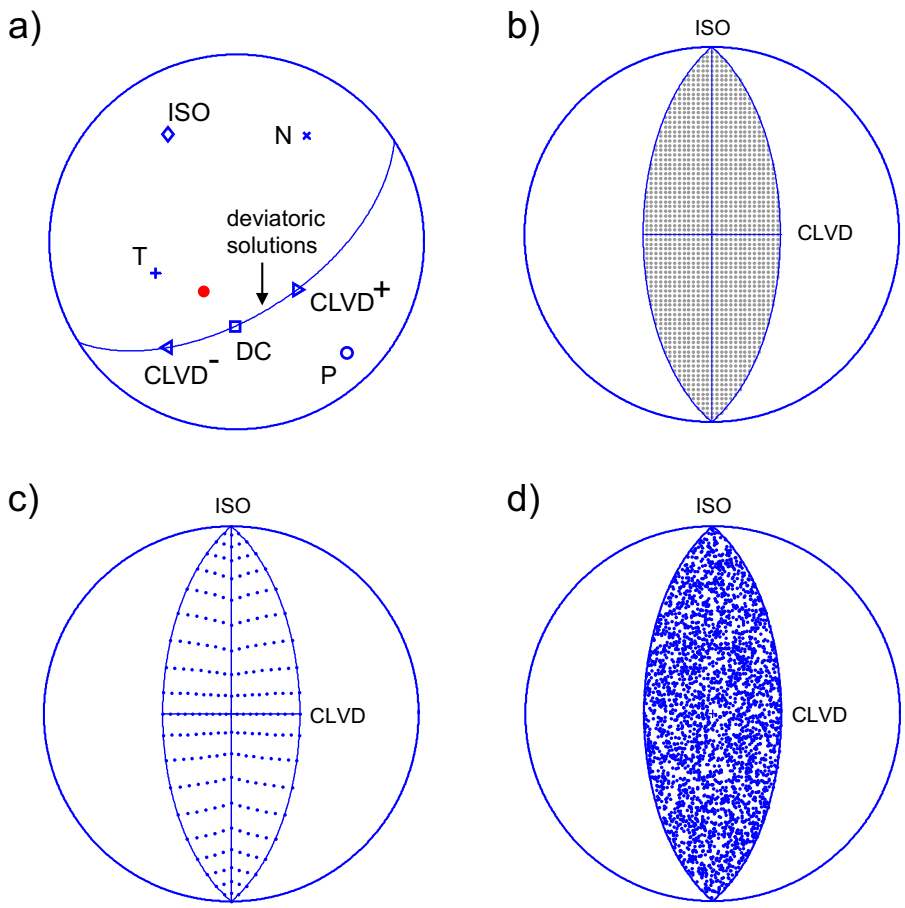

Fig. 8 The Riedesel–Jordan source-type plot. **a** The original compact plot proposed by Riedesel and Jordan (1989) displaying both the orientation of the moment tensor eigenvectors (*P*, *T* and *N* axes), basic source types (ISO, CLVD, DC) and the position of the studied moment tensor (*red dot*). **b**–**d** A modified Riedesel–Jordan plot proposed by Chapman and Leaney (2012). The *dashed area* in **b** shows the area of admissible positions of sources. The *dots* in **c** show a regular grid in C_{ISO} and C_{CLVD} from −1 to 1 with step of 0.1. The *dots* in **d** show 3,000 sources defined by the moment tensors with randomly generated eigenvalues normalized by the Euclidean norm of **M**. Plot **d** indicates that the distribution of sources is uniform

$$\mathbf{e}^{-}_{\mathrm{CLVD}} = \sqrt{\frac{2}{3}}\left(\frac{1}{2}\mathbf{e}_1 + \frac{1}{2}\mathbf{e}_2 - \mathbf{e}_3\right) = \left(0, -\frac{1}{2}, \frac{\sqrt{3}}{2}\right)^T. \quad (50)$$

The basic properties of this projection are exemplified in Fig. 8c, d: Fig. 8c shows the mapping of a regular grid in C_{ISO} and C_{CLVD} calculated using Eqs. (6–10), and Fig. 8d indicates that the PDF of sources with eigenvalues M_1, M_2 and M_3 randomly distributed over the lune is uniform. Obviously, if the moment tensors are normalized using other than the Euclidean norm, the PDF of sources in the Riedesel–Jordan plot will be non-uniform, for example, when points uniformly distributed on the cube are projected on the sphere.

As discussed in Section 5.2, the coordinate system in the decomposition with the Euclidean norm meets difficulties. The ISO and DC axes lie in the source-type space, but the CLVD axis (with the CLVD's major dipole oriented along the N axis) lies outside this space. As a consequence, the CLVD does not lie in the source-type plot and the CLVD scale factor can never attain a value of ±1 but only of ±1/4 at the most. Another difficulty with this decomposition mentioned in Section 5.2 is that the tensile crack is characterized by a non-zero DC component.

The above-mentioned problems with the CLVD scaling can be removed if the CLVD axis in the Riedesel–Jordan plot is rescaled by the multiplication factor of 4. Consequently, base tensors $\mathbf{E}^{+}_{\mathrm{CLVD}}$ or $\mathbf{E}^{-}_{\mathrm{CLVD}}$ defined in Eq. (5) will attain values of $C_{\mathrm{CLVD}}=\pm 1$, similarly as in the standard decomposition. In addition, it might appear to be more practical to stretch the CLVD axis and to transform the lune plot into a circular plot.

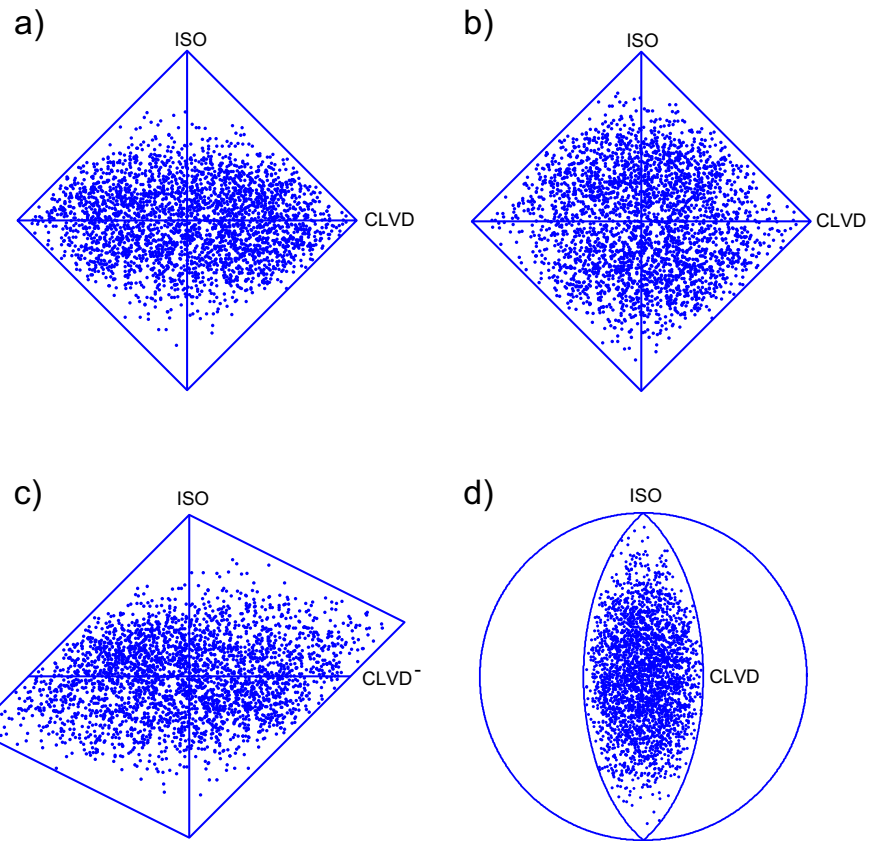

Fig. 9 Distribution of random sources in four different source-type plots. **a** The diamond CLVD–ISO plot using the standard decomposition (see Section 3.1), **b** the diamond CLVD–ISO plot using the simplified decomposition (see Section 5.1), **c** the Hudson's skewed diamond plot (see Section 6.1), and **d** the Riedesel–Jordan plot (see Section 6.2). The *dots* show 3,000 sources defined by the moment tensors with randomly generated components in the interval from −1 to 1. The distribution of sources is non-uniform for all source-type plots

6.3 Analysis of moment tensor uncertainties using source-type plots

Source-type plots are often used for assessing uncertainties of the ISO, DC and CLVD components of moment tensors. In this section, we compare several source-type plots and discuss how the errors are projected into them.

The idea behind using the source-type plots for assessing errors is simple. The moment tensor is not plotted just as one point corresponding to an optimum solution but as a cluster of acceptable solutions. The size of the cluster measures uncertainties of the solution. Obviously, this approach is reasonable if the same size of a cluster corresponds to the same uncertainties independently of the position of the cluster in the source-type plot. Most seismologists assume that this property is uniquely satisfied in the skewed diamond plot because randomly generated eigenvalues cover uniformly this plot (Fig. 7d). However, this is not quite true for two reasons. Firstly, if the appropriate norm of eigenvalues is applied, the other source-type plots also display a uniform PDF for randomly generated eigenvalues (see Sections 6.1 and 6.2). Secondly, when the uncertainties of the individual moment tensor components are analysed, the moment tensor is not in the diagonal form. After diagonalizing the moment tensor, the errors are projected into the errors of eigenvalues in a rather complicated way. This is demonstrated in Fig. 9, which shows sources with moment tensors having all six independent components randomly distributed with a uniform probability in the interval from −1 to 1. The figure indicates that some source types are quite rare, in particular, sources with high explosive or implosive components. This observation is common for all source-type plots and confirms the well-known fact that the

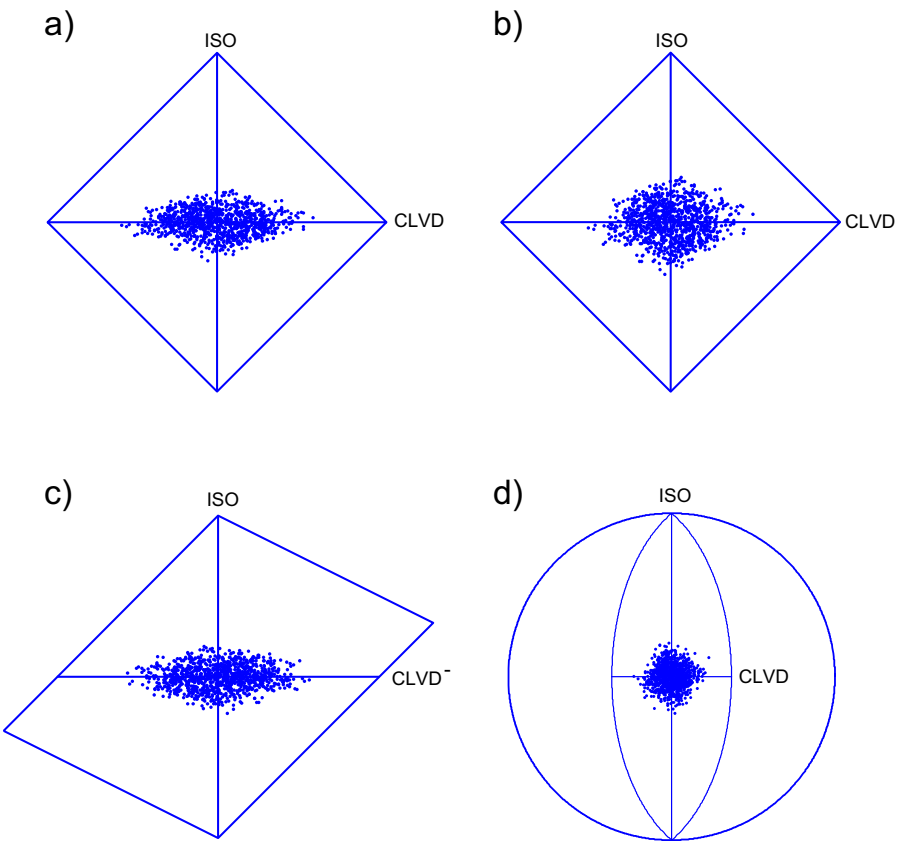

Fig. 10 Distribution of pure DC sources contaminated by random noise in four different source-type plots. **a** The diamond CLVD–ISO plot using the standard decomposition, **b** the diamond CLVD–ISO plot using the simplified decomposition, **c** the Hudson's skewed diamond plot, and **d** the Riedesel–Jordan plot. The *dots* show 1,000 DC sources defined by the elementary tensor $\mathbf{E}_{DC}$ (see Eq. 4) and contaminated by noise with a uniform distribution between −0.25 and 0.25. The noise is superimposed to all tensor components

distribution of eigenvalues for random matrices is not uniform (Mehta 2004).

More realistic sources are modelled in Figs. 10 and 11: the pure DC and ISO sources defined by tensors $\mathbf{E}_{DC}$ and $\mathbf{E}_{ISO}$ using Eq. (5) are contaminated by random noise with a uniform distribution in the interval from −0.25 to 0.25. The noise is superimposed to all six tensor components, and 1,000 random moment tensors are generated. As expected, the randomly generated moment tensors form clusters, but their shape is different for different projections, and their size depends also on the type of source. For the DC source (Fig. 10), the maximum PDF is in the centre of the cluster which coincides with the position of the uncontaminated source. In the diamond CLVD–ISO plot (Fig. 10a) and Hudson's skewed diamond plot (Fig. 10c), the cluster is asymmetric, being stretched along the CLVD axis. A more symmetric cluster is produced in the diamond CLVD–ISO plot (Fig. 10b) when the simplified decomposition is applied (see Section 5.1) and in the Riedesel–Jordan plot (Fig. 10d). However, the symmetry of the cluster is apparent in the Riedesel–Jordan plot because the CLVD and ISO axes are of different lengths. A significantly higher scatter of the CLVD components compared to the ISO components in the moment tensor inversions has been observed and discussed also in Vavryčuk (2011). For the pure ISO source (Fig. 11), the clusters are smaller than for the DC source, and the maximum PDF is outside the position of the uncontaminated source. This means that the ISO percentage is systematically underestimated due to the errors of the inversion for highly explosive or implosive sources. This is interesting and should be taken into account when interpreting real observations.

Finally, we conclude that the comparison of various source-type plots did not prove a clear preference for the Hudson skewed diamond plot or for any other plot in error interpretations. A uniform probability of moment eigenvalues in the source-type plots does not provide any specific advantage in the error analysis. Moment tensors displaying the same uncertainties can project into clusters of a different size.

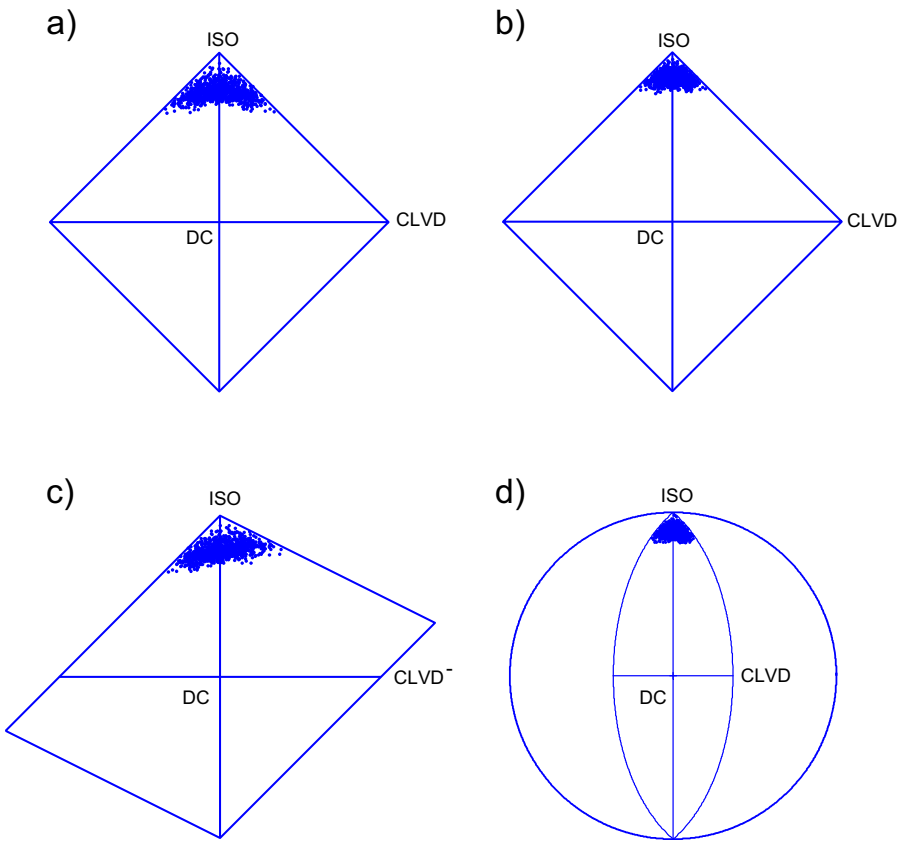

Fig. 11 The same as Fig. 10 but for the pure ISO source contaminated by random noise

7 Discussion

The standard decomposition into ISO, DC and CLVD components described in Section 3 and its modification proposed in Section 5.1 are the only decompositions which define the base vectors (tensors) within the source-type space. This property implies that the individual parts of the decomposed moment tensor are uniquely defined and can exist as individual source types. Consequently, the base vectors are mapped inside the source-type plot. Since the source-type space is a wedge in 3-D space, the base vectors of the source-type space cannot form an orthogonal basis.

The base vectors of other decompositions such as the decomposition into the ISO and three DCs, the ISO and the major and minor DCs or the ISO and two DCs with the same T axes do not form a vector basis inside the source-type space. This is somewhat inconvenient because some of the decomposed parts of the moment tensors are not defined in the source-type space and thus cannot exist independently as individual types of source. This also applies to the approach of Chapman and Leaney (2012), who proposed the ISO, DC and CLVD decomposition using the Euclidean norm and the CLVD with the major dipole oriented along the N axis. As a consequence, relative scale factor C^*_{CLVD} can never attain the value of ±1 for any moment tensor but only ±1/4. This decomposition has also some other undesirable properties, for example, pure tensile faulting in isotropic media yields a non-zero DC component. This is against physical intuition since the DC is usually considered to be a measure of the amount of shear faulting in seismic sources.

In analysing the general moment tensors, we face the following key problems: how to define the scalar seismic moment and what is the most appropriate norm of the moment tensor in the moment tensor decompositions. The standard decomposition defines the scalar moment as the sum of spectral norms of the individual moment tensor components. In principle, the scalar moment could be defined also as the spectral norm of complete moment tensor **M**. However, this definition introduces difficulties in the moment tensor decomposition because it can produce the sum of the ISO, DC and CLVD relative scale factors higher than 1 (provided the ISO and CLVD parts are of opposite signs). Another possibility is using the Euclidean norm for defining the scalar moment and consequently for decomposing the moment tensors. However, applying the Euclidean norm is also tricky. This norm is appropriate for orthogonal spaces, for example, when working in the 6-D space of full moment tensors. But the source-type space of ordered eigenvalues of moment tensors is a wedge of the full 3-D space, and thus it is not orthogonal.

Different approaches to the moment tensor decomposition project into constructing various source-type plots used in interpretations. We show that the Hudson skewed diamond plot can be introduced in a much simpler way than originally proposed by Hudson et al. (1989). The plot can readily be constructed using the ISO and CLVD components scaled to the spectral norm of moment tensor **M**. The plot conserves the uniform distribution probability of moment eigenvalues, but the analysis indicates that it does not provide any essential advantage for error interpretations. Interestingly, also other source-type plots such as the diamond plot or the Riedesel–Jordan lune plot conserve the uniform distribution probability of moment eigenvalues if the appropriate norm is adopted. But again, this provides no clear benefit in the error analysis because the errors of the eigenvectors and eigenvalues of the moment tensors cannot be easily separated. Hence, the source-type plots should be viewed as a rather simple tool for visualizing the basic classification of sources. A detailed and accurate analysis of seismic sources should always be performed using the complete moment tensors. For these reasons, the most straightforward and comprehensible approach for the first source-type interpretations is probably the simple diamond CLVD–ISO plot.

Acknowledgments I wish to thank Jan Šílený and an anonymous reviewer for their detailed and constructive comments which helped to improve the paper significantly. The study was supported by the Grant Agency of the Czech Republic, Grant No. P210/12/1491.

Appendix A. Calculation of moment tensor M from the scalar moment M and the ISO, DC and CLVD scale factors

The eigenvalues of moment tensor **M** are calculated from scale factors C_{ISO}, C_{DC}, C_{CLVD} and scalar seismic moment M defined in Eqs. (6–10) using the following simple formulas:

for $C_{\mathrm{CLVD}} \geq 0$

$$\begin{aligned} M_1 &= M(C_{\mathrm{ISO}} + C_{\mathrm{DC}} + C_{\mathrm{CLVD}}), \\ M_2 &= M\left(C_{\mathrm{ISO}} - \frac{1}{2}C_{\mathrm{CLVD}}\right), \\ M_3 &= M\left(C_{\mathrm{ISO}} - C_{\mathrm{DC}} - \frac{1}{2}C_{\mathrm{CLVD}}\right), \end{aligned} \tag{A1}$$

and for $C_{\mathrm{CLVD}} < 0$

$$\begin{aligned} M_1 &= M\left(C_{\mathrm{ISO}} + C_{\mathrm{DC}} - \frac{1}{2}C_{\mathrm{CLVD}}\right), \\ M_2 &= M\left(C_{\mathrm{ISO}} - \frac{1}{2}C_{\mathrm{CLVD}}\right), \\ M_3 &= M(C_{\mathrm{ISO}} - C_{\mathrm{DC}} + C_{\mathrm{CLVD}}). \end{aligned} \tag{A2}$$

Appendix B. The ISO, DC and CLVD decomposition of the source tensor

Source tensor **D** of the shear-tensile model

$$\begin{aligned} \mathbf{D} &= \frac{uS}{2}(\mathbf{ns} + \mathbf{sn}) \\ &= \frac{uS}{2}\begin{bmatrix} 2n_1s_1 & n_1s_2 + n_2s_1 & n_1s_3 + n_3s_1 \\ n_1s_2 + n_2s_1 & 2n_2s_2 & n_2s_3 + n_3s_2 \\ n_1s_3 + n_3s_1 & n_2s_3 + n_3s_2 & 2n_3s_3 \end{bmatrix} \end{aligned} \tag{B1}$$

has the following diagonal form (see Vavryčuk 2005, his Appendix B):

$$\mathbf{D}^{diag} = \frac{uS}{2}\begin{bmatrix} \mathbf{n}\cdot\mathbf{s} + 1 & 0 & 0 \\ 0 & 0 & 0 \\ 0 & 0 & \mathbf{n}\cdot\mathbf{s} - 1 \end{bmatrix}, \tag{B2}$$

where $\mathbf{n}\cdot\mathbf{s}$ is the scalar product of two unit vectors **n** and **s**. Vector **n** is the fault normal, and **s** is the direction of the slip vector. The maximum eigenvalue $D_1 = \frac{uS}{2}(\mathbf{n}\cdot\mathbf{s} + 1)$ is positive or zero, the minimum eigenvalue $D_3 = \frac{uS}{2}(\mathbf{n}\cdot\mathbf{s} - 1)$ is negative or zero. Using Eqs. (6–10) we obtain

$$D_{\mathrm{ISO}} = \frac{1}{3}(D_1 + D_2 + D_3) = \frac{1}{3}uS(\mathbf{n}\cdot\mathbf{s}), \tag{B3}$$

$$D_{\mathrm{CLVD}} = \frac{2}{3}(D_1 + D_3 - 2D_2) = \frac{2}{3}uS(\mathbf{n}\cdot\mathbf{s}), \tag{B4}$$

$$\begin{aligned} D_{\mathrm{DC}} &= \frac{1}{2}(D_1 - D_3 - |D_1 + D_3 - 2D_2|) \\ &= \frac{1}{2}uS(1 - |\mathbf{n}\cdot\mathbf{s}|), \end{aligned} \tag{B5}$$

$$\begin{aligned} D &= \frac{1}{2}(|D_{\mathrm{ISO}}| + |D_{\mathrm{CLVD}}| + D_{\mathrm{DC}}) \\ &= \frac{1}{2}uS(1 + |\mathbf{n}\cdot\mathbf{s}|), \end{aligned} \tag{B6}$$

so the scale factors C_{ISO}, C_{DC} and C_{CLVD} read

$$\begin{bmatrix} C_{\mathrm{ISO}} \\ C_{\mathrm{CLVD}} \\ C_{\mathrm{DC}} \end{bmatrix} = \frac{1}{3(1 + |\mathbf{n}\cdot\mathbf{s}|)}\begin{bmatrix} 2\mathbf{n}\cdot\mathbf{s} \\ 4\mathbf{n}\cdot\mathbf{s} \\ 3(1 - |\mathbf{n}\cdot\mathbf{s}|) \end{bmatrix}. \tag{B7}$$

It follows from Eqs. (B3-B4) that the ISO/CLVD ratio is 1/2 independently of the slope angle α, calculated as $\sin\alpha = \mathbf{n}\cdot\mathbf{s}$ (see Vavryčuk 2011).

References

Aki K, Richards PG (2002) Quantitative seismology. University Science, Sausalito

Ampuero J-P, Dahlen FA (2005) Ambiguity of the moment tensor. Bull Seismol Soc Am 95:390–400

Ben-Zion Y (2001) On quantification of the earthquake source. Seismol Res Lett 72:151–152

Ben-Zion Y (2003) Key formulas in earthquake seismology. In: Lee WHK et al (eds) International handbook of earthquake and engineering seismology. Academic, Amsterdam, pp 1857–1875

Bowers D, Hudson JA (1999) Defining the scalar moment of a seismic source with a general moment tensor. Bull Seismol Soc Am 89(5):1390–1394

Burridge R, Knopoff L (1964) Body force equivalents for seismic dislocations. Bull Seismol Soc Am 54:1875–1888

Chapman CH, Leaney WS (2012) A new moment-tensor decomposition for seismic events in anisotropic media. Geophys J Int 188:343–370

Dufumier H, Rivera L (1997) On the resolution of the isotropic component in moment tensor. Geophys J Int 131:595–606

Dziewonski AM, Chou T-A, Woodhouse JH (1981) Determination of earthquake source parameters from waveform data for studies of global and regional seismicity. J Geophys Res 86:2825–2852

Hudson JA, Pearce RG, Rogers RM (1989) Source type plot for inversion of the moment tensor. J Geophys Res 94:765–774

Jost ML, Herrmann RB (1989) A student's guide to and review of moment tensors. Seismol Res Lett 60:37–57

Julian BR, Miller AD, Foulger GR (1997) Non-double-couple earthquake mechanisms at the Hengill–Grensdalur volcanic complex, southwest Iceland. Geophys Res Lett 24:743–746

Julian BR, Miller AD, Foulger GR (1998) Non-double-couple earthquakes 1: theory. Rev Geophys 36:525–549

Kawasaki I, Tanimoto T (1981) Radiation patterns of body waves due to the seismic dislocation occurring in an anisotropic source medium. Bull Seismol Soc Am 71:37–50

Knopoff L, Randall MJ (1970) The compensated linear-vector dipole: a possible mechanism for deep earthquakes. J Geophys Res 75:4957–4963

Kuge K, Lay T (1994) Data-dependent non-double-couple components of shallow earthquake source mechanisms: effects of waveform inversion instability. Geophys Res Lett 21:9–12

Mehta ML (2004) Random matrices. Elsevier, Amsterdam

Miller AD, Foulger GR, Julian BR (1998) Non-double-couple earthquakes 2: observations. Rev Geophys 36:551–568

Minson SE, Dreger DS, Bürgmann R, Kanamori H, Larson KM (2007) Seismically and geodetically determined nondouble-couple source mechanisms from the 2000 Miyakejima volcanic earthquake swarm. J Geophys Res 112:B10308, doi:10.1029/2006JB004847

Riedesel MA, Jordan TH (1989) Display and assessment of seismic moment tensors. Bull Seismol Soc Am 79:85–100

Roessler D, Ruempker G, Krueger F (2004) Ambiguous moment tensors and radiation patterns in anisotropic media with applications to the modeling of earthquake mechanisms in W-Bohemia. Stud Geophys Geod 48:233–250

Roessler D, Krueger F, Ruempker G (2007) Retrieval of moment tensors due to dislocation point sources in anisotropic media using standard techniques. Geophys J Int 169:136–148

Ross AG, Foulger GR, Julian BR (1996) Non-double-couple earthquake mechanisms at the Geysers geothermal area, California. Geophys Res Lett 23:877–880

Rudajev V, Šílený J (1985) Seismic events with non-shear components, II. Rockbursts with implosive source component. Pure Appl Geophys 123:17–25

Šílený J, Milev A (2008) Source mechanism of mining induced seismic events—resolution of double couple and non double couple models. Tectonophys 456(1–2):3–15

Sipkin SA (1986) Interpretation of non-double-couple earthquake mechanisms derived from moment tensor inversion. J Geophys Res 91:531–547

Silver PG, Jordan TH (1982) Optimal estimation of the scalar seismic moment. Geophys J Roy Astr Soc 70:755–787

Stierle E, Vavryčuk V, Šílený J, Bohnhoff M (2014a) Resolution of non-double-couple components in the seismic moment tensor using regional networks—I: a synthetic case study. Geophys J Int 196(3):1869–1877

Stierle E, Bohnhoff M, Vavryčuk V (2014b) Resolution of non-double-couple components in the seismic moment tensor using regional networks - II: application to aftershocks of the 1999 Mw 7.4 Izmit earthquake. Geophys J Int 196(3):1878–1888

Tape W, Tape C (2012a) A geometric setting for moment tensors. Geophys J Int 190:476–498

Tape W, Tape C (2012b) A geometric comparison of source-type plots for moment tensors. Geophys J Int 190:499–510

Vavryčuk V (2001) Inversion for parameters of tensile earthquakes. J Geophys Res 106(B8):16.339–16.355. doi:10.1029/2001JB000372

Vavryčuk V (2004) Inversion for anisotropy from non-double-couple components of moment tensors. J Geophys Res 109, B07306. doi:10.1029/2003JB002926

Vavryčuk V (2005) Focal mechanisms in anisotropic media. Geophys J Int 161:334–346. doi:10.1111/j.1365-246X.2005.02585.x

Vavryčuk V (2011) Tensile earthquakes: theory, modeling, and inversion. J Geophys Res 116:B12320, doi:10.1029/2011JB008770

Vavryčuk V (2013) Is the seismic moment tensor ambiguous at a material interface? Geophys J Int 194:395–400. doi:10.1093/gji/ggt084

Vavryčuk V, Bohnhoff M, Jechumtálová J, Kolář P, Šílený J (2008) Non-double-couple mechanisms of micro-earthquakes induced during the 2000 injection experiment at the KTB site, Germany: a result of tensile faulting or anisotropy of a rock? Tectonophys 456:74–93. doi:10.1016/j.tecto.2007.08.019

Vernik L, Liu X (1997) Velocity anisotropy in shales: a petrological study. Geophysics 62:521–532

Zhu L, Ben-Zion Y (2013) Parameterization of general seismic potency and moment tensors for source inversion of seismic waveform data. Geophys J Int 194:839–843. doi:10.1093/gji/ggt137